

Grad's 13 moments to the rescue of compressible lattice Boltzmann methods

Andrea Parmigiani,¹ Christophe Coreixas,² Joël Beny,² and Jonas Latt^{1,2,*}

¹*FlowKit-Numeca Group Ltd, Route d'Oron 2, 1010 Lausanne, Switzerland*

²*Department of Computer Science, University of Geneva, 1204 Geneva, Switzerland*

(Dated: October 11, 2024)

A double-distribution-function based lattice Boltzmann method (DDF-LBM) is proposed for the simulation of polyatomic gases in the supersonic regime. The model relies on an extended equilibrium state that is constructed to mimic Grad's 13 moments of the Maxwell-Boltzmann distribution. This allows the correct simulation of thermal, compressible flows with only 39 discrete velocities. The stability of this BGK-LBM is reinforced by relying on Knudsen-number-dependent relaxation times that are computed analytically. Hence, high-Reynolds number, supersonic flows can be simulated in an efficient and elegant manner. While the 1D Riemann problem shows the ability of the proposed approach to handle discontinuities in the zero-viscosity limit, the simulation of the flow past a NACA0012 airfoil (Mach number $Ma = 1.5$, Reynolds number $Re = 10^4$) confirms the excellent behavior of this model in a turbulent and supersonic regime. The proposed model is substantially more efficient than previous models and opens up a whole new world of compressible flow applications that can be realistically tackled with a purely LB approach.

Introduction. The lattice Boltzmann method (LBM) is a popular numerical scheme capable of computing solutions of the Boltzmann equation (BE) in a regime of small deviations from the local equilibrium state. In the BE, the statistical behavior of gas molecules is described by the continuous velocity distribution function $f(\mathbf{x}, \boldsymbol{\xi}, t)$ that depends on the spatial position \mathbf{x} , the molecular velocity $\boldsymbol{\xi}$ and time t ¹. In the LB scheme, the space of molecular velocities is discretized: the velocity distribution function is replaced by a discrete set of V populations $f_i(\mathbf{x}, t)$, $i = 0 \cdots V - 1$ standing for the statistics of molecules at discrete velocities $\boldsymbol{\xi}_i$. Increasing the number of discrete velocities, and thus populations, typically allows to extend the physical range of validity of the scheme².

Although LBM describes intrinsically compressible fluids, it has arguably achieved its most striking successes in the realm of incompressible fluid flow^{3,4} and has until recently struggled to establish itself as a realistic alternative for the simulation of compressible and/or high Mach number flows⁵. While simulating fluid flow may seem as easy as adding discrete velocities to the LBM scheme, these so-called multi-speed approaches rapidly lead to schemes with a large number of velocities, which translate in an impractically large number of degrees of freedom per mesh cell. In addition to that, these models are usually limited by numerical instabilities⁶ if the numerical scheme is not modified⁵, or if a more sophisticated collision model is not adopted^{7,8}.

As a popular workaround, the momentum and energy equations can be split and solved separately, as they individually require a substantially smaller set of velocities^{9,10}. Further computational efficiency is achieved by solving the energy equation with a traditional finite-difference, finite-volume, or finite-element scheme^{11–13}. These solutions introduce however new problems of their own making in the shape of coupling instabilities.

Another highly promising path has been recently proposed which improves numerical stability by representing

the equilibrium state of the populations by a more elaborate term than the traditional polynomial expansion of the Maxwell-Boltzmann distribution. Instead, an exponential equilibrium distribution is computed on each cell and at each time step by solving a set of non-linear equations, subject to the five scalar constraints of mass, momentum, and energy conservation^{14,15}. Among DDF approaches based on the collide-and-stream algorithm, this is to our knowledge one of the most promising proposition in the current literature capable of achieving good numerical stability for non-trivial, transonic and supersonic flows. The computational cost of this methodology is however very high, as this method requires typically two populations composed of 343 velocities each, compared to the conventional 19 or 27 velocities needed to simulate weakly compressible and athermal flows. In addition, it relies on the entropic collision model that consists in minimizing the H-function, on every single grid point and at every time iteration, in order to get more stable simulations. This eventually leads to a further non-negligible overhead.

In this Rapid Communication, we extend the above method by computing an exponential equilibrium subject to 13 instead of 5 constraints, following an idea originally evoked in the PhD manuscript of Frapolli¹⁶. In this manner, the behavior of the macroscopic flow variables, which are related to the moments of the particle populations, can be adequately represented using as few as 39 discrete velocities by putting more effort on the equilibrium instead of the lattice. This is explained by the fact that the desired moments of the distribution are strictly enforced with the help of a numerical solver. Hence, they no longer depend on the choice of a sophisticated discrete velocity stencil, or at least, the dependency is highly reduced. Numerical tests shown in this article confirm that the model exhibits both a good stability and accuracy with this reduced velocity set. Compared with the 5-constraint model, the memory requirements are thus reduced by an order of magnitude, and the computa-

tional cost is diminished correspondingly. In contrast to the entropic collision model, we prefer to rely on BGK operators that are stabilized by identifying areas of the simulation domain where the departure from equilibrium is high. In doing so, relaxation times can be adjusted to damp high-order modes, which efficiently leads to stable and accurate simulation of supersonic flows with discontinuities. Consequently, the proposed model combines the elegance of a fully LB model for compressible flows with a level of robustness and efficiency.

The model. The Maxwell-Boltzmann distribution

$$f^{eq} = \frac{\rho}{(2\pi T)^{D/2}} \exp\left(-\frac{(\boldsymbol{\xi} - \mathbf{u})^2}{2T}\right), \quad (1)$$

describes an equilibrium state and yields an exact solution of the Boltzmann equation. The macroscopic density ρ , velocity \mathbf{u} and temperature T are equal to or directly linked with velocity moments of the probability distribution function. A macroscopic variable is a collision invariant, and thus a conserved quantity, if the corresponding moment of the distribution function f and of the equilibrium state f^{eq} are equal. It is easily verified that for the continuum Maxwell-Boltzmann distribution, density, velocity, and total energy are conserved quantities.

In the discrete LB method, the equilibrium populations f_i^{eq} are a mere approximation of the Maxwell-Boltzmann distribution, but most LB models guarantee the correct definition of conserved macroscopic quantities after the velocity space discretization. To achieve this goal, the most common methodology is to rely on Gauss-Hermite quadrature². In this case, the match between moments and macroscopic variable is nothing else than a statement of orthogonality between Hermite polynomials. However, the number of discrete velocities required to express appropriate orthogonality relations and include effects of energy conservation can be prohibitively large (at least 100 velocities in 3D). As an alternative, other authors proposed to manually enforce conservation laws by constantly recomputing the equilibrium by a root-finding procedure subject to appropriate constraints¹⁴.

Beyond conserved quantities, it is however necessary for the moments of the discrete equilibrium to yield the same value as the corresponding moments of the Maxwell-Boltzmann distribution in order to recover the desired physical behavior. We now provide a short reasoning for this argument, and compute the order of the moments that need to be recovered exactly to produce Navier-Stokes-Fourier (NSF) level physics. The compressible NSF equations read

$$\begin{aligned} \partial_t \rho + \partial_\chi(\rho u_\chi) &= 0, \\ \partial_t(\rho u_\alpha) + \partial_\beta(\rho u_\alpha u_\beta + p \delta_{\alpha\beta}) &= \partial_\beta(\Pi_{\alpha\beta}), \\ \partial_t(\rho E) + \partial_\alpha((\rho E + p)u_\alpha) &= \partial_\alpha(\Phi_\alpha), \end{aligned} \quad (2)$$

where the index repetition implies the Einstein summation rule. The viscous stress tensor $\Pi_{\alpha\beta}$ is defined as

$$\Pi_{\alpha\beta} = \mu(S_{\alpha\beta} - \frac{2}{D}\partial_\chi u_\chi \delta_{\alpha\beta}) + \mu_b \partial_\chi u_\chi \delta_{\alpha\beta},$$

with $S_{\alpha\beta} = \partial_\alpha u_\beta + \partial_\beta u_\alpha$, and μ and $\mu_b = (2/D - 1/C_v)\mu$ being the dynamic and bulk viscosity respectively. D is the number of physical dimensions, $C_v = 1/(\gamma - 1)$ is the heat capacity at constant volume, γ is the heat capacity ratio, and E is the total energy. Dissipative effects in the total energy equation are gathered in the term

$$\Phi_\alpha = -\lambda \partial_\alpha T + u_\beta \Pi_{\alpha\beta},$$

which accounts for both the Fourier heat flux (λ is the heat conductivity), and the viscous heat dissipation. In case of a calorically perfect gas, this system is closed by the following equation of state: $E = \frac{1}{2}u^2 + C_v T$.

The moments of the Maxwell-Boltzmann distribution can be written as

$$M_{pqr}^{\text{MB}} = \int \xi_x^p \xi_y^q \xi_z^r f^{eq} d\boldsymbol{\xi}. \quad (3)$$

For comparison with macroscopic equations, it is more convenient to write them in the following compact form:

$$\begin{aligned} M_0^{\text{MB}} &= \rho, \\ M_{1,\alpha}^{\text{MB}} &= \rho u_\alpha, \\ M_{2,\alpha\beta}^{\text{MB}} &= \rho u_\alpha u_\beta + \rho T \delta_{\alpha\beta}, \\ M_{3,\alpha\beta\gamma}^{\text{MB}} &= \rho u_\alpha u_\beta u_\gamma + \rho T [u_\alpha \delta_{\beta\gamma}]_{cyc}, \\ M_{4,\alpha\beta\gamma\chi}^{\text{MB}} &= \rho u_\alpha u_\beta u_\gamma u_\chi + \rho T [u_\alpha u_\beta \delta_{\gamma\chi}]_{cyc} + \rho T^2 [\delta_{\alpha\beta} \delta_{\gamma\chi}]_{cyc}, \end{aligned} \quad (4)$$

where $\alpha, \beta, \gamma, \chi$ represent space coordinates (x, y or z). The subscript *cyc* labels a cyclic permutation without repetition. As an example,

$$T^2 [\delta_{\alpha\beta} \delta_{\gamma\chi}]_{cyc} = T^2 (\delta_{\alpha\beta} \delta_{\gamma\chi} + \delta_{\alpha\gamma} \delta_{\beta\chi} + \delta_{\alpha\chi} \delta_{\beta\gamma}).$$

Now, the NSF equations are easily rewritten in terms of equilibrium moments as follows:

$$\partial_t(M_0^{\text{MB}}) + \partial_\beta(M_{1,\beta}^{\text{MB}}) = 0, \quad (5)$$

$$\partial_t(M_{1,\alpha}^{\text{MB}}) + \partial_\beta(M_{2,\alpha\beta}^{\text{MB}}) \propto \partial_t(M_{2,\alpha\beta}^{\text{MB}}) + \partial_\gamma(M_{3,\alpha\beta\gamma}^{\text{MB}}), \quad (6)$$

$$\partial_t(M_{2,\alpha\alpha}^{\text{MB}}) + \partial_\beta(M_{3,\alpha\alpha\beta}^{\text{MB}}) \propto \partial_t(M_{3,\alpha\alpha\beta}^{\text{MB}}) + \partial_\beta(M_{4,\alpha\alpha\beta\chi}^{\text{MB}}). \quad (7)$$

Here, the diffusive RHS terms have been related to equilibrium moments through the Chapman-Enskog expansion, where the time derivatives are usually replaced using Euler-level equations for $M_{2,\alpha\beta}^{\text{MB}}$ and $M_{3,\alpha\beta\gamma}^{\text{MB}}$. From this, it is clear that moments of f^{eq} up to $n = 4$ are necessary to recover NSF equations (2).

Consequently, the matching conditions between discrete and continuous moments read:

$$\sum_i f_i^{eq} \xi_x^p \xi_y^q \xi_z^r = M_{pqr}^{\text{MB}}. \quad (8)$$

with $p + q + r = n$. These conditions are enforced using the following (exponential) discrete equilibrium:

$$f_i^{eq} = \exp[-(1 + \sum_{p,q,r} \lambda M_{pqr}^{\text{MB}} \xi_x^p \xi_y^q \xi_z^r)], \quad (9)$$

where $\lambda_{M_{pqr}^{MB}}$ are Lagrange multipliers whose purpose is to match the following constraints:

$$G_{pqr} = \sum_i f_i^{eq} \xi_x^p \xi_y^q \xi_z^r - M_{pqr}^{MB} = 0, \quad (10)$$

This particular form of the equilibrium (9) is obtained via the principle of maximum entropy, considering the following H -function $H = \sum_i f_i \ln f_i$ ^{17,18}, and under the constraints (10).

It is useful to note that contrarily to standard LB models, the above equilibrium does not explicitly introduce lattice weights. The latter originates from the quadrature used for the standard construction of the lattice and its corresponding polynomial equilibrium. Such a methodology is not carried anymore in the present context, hence the solution procedure is quadrature-free.

In case of the NSF equations, the moments should ideally be matched up to fourth order. In this first study, we restrict ourselves however to Grad's 13 moments, while forthcoming studies will consider higher-order moments (R26, R45, etc)¹⁹. Here, the discrete equilibrium reads

$$f_i^{eq} = \rho \exp \left(\lambda_0 + \lambda_{1,\alpha} \xi_{i,\alpha} + \lambda_{2,\alpha\beta} \xi_{i,\alpha} \xi_{i,\beta} + \lambda_{3,\alpha} \xi_{i,\alpha} |\xi_i|^2 \right). \quad (11)$$

Here, λ_2 is a symmetric tensor with 6 independent variables. Thus, the equilibrium depends only on 13 unknown variables, which are matched with the following 13 constraints:

$$M_0^{eq} = \sum_i f_i^{eq} = \rho \quad (12)$$

$$M_{1,\alpha}^{eq} = \sum_i f_i^{eq} \xi_{i,\alpha} = \rho u_\alpha \quad (13)$$

$$M_{2,\alpha\beta}^{eq} = \sum_i f_i^{eq} \xi_{i,\alpha} \xi_{i,\beta} = \rho u_\alpha u_\beta + \rho T \delta_{\alpha\beta} \quad (14)$$

$$M_{3,\alpha\beta\beta}^{eq} = \sum_i f_i^{eq} \xi_{i,\alpha} |\xi_i|^2 = (2\rho E^{tr} + 2\rho T) u_\alpha \quad (15)$$

where the total translational energy E^{tr} reads $E^{tr} = DT + \rho u^2$. These equations express the conservation of mass and momentum, and enforce a desired form for the pressure tensor (which includes the conservation law for the translational energy) and the contracted heat flux tensor. To further extend the above approach to polyatomic gases, one can rely on a second set of populations g_i described by the following equilibrium^{20,21}

$$g_i^{eq} = (2C_v - D) T f_i^{eq}, \quad (16)$$

that is built on top of f_i^{eq} .

Numerical method. The above model is based on the collide-and-stream algorithm in D3Q39 velocity space². For the collision step, each cell first computes the macroscopic variables (ρ , \mathbf{u} , T and E^{tr}) and evaluates the moments, Eq. (12). Then, the 13 unknown variables λ_i are computed by plugging Eq. (11) into equations (10) and solving the system (we used a standard multivariate

Newton-Raphson root solver²²). Once the f_i^{eq} are known, g_i^{eq} is computed using Eq. (16). Adopting the BGK collision model, post-streaming populations are finally computed using the standard collide-and-stream algorithm, formulated in lattice units:

$$h_i(\mathbf{x} + \boldsymbol{\xi}_i, t + 1) = h_i(\mathbf{x}, t) - \frac{1}{\tau_h} \left(h_i - h_i^{(eq)} \right) (\mathbf{x}, t), \quad (17)$$

where h is the population, representing $h = f$ or $h = g$. In addition, the Prandtl number could be adjusted using either the quasi-equilibrium¹⁵, or a more standard approach⁸. This was not implemented in the present publication, which limits the simulations to $Pr = 1$.

In case better stability is required, the relaxation time is made Knudsen-number dependent. This is done by locally computing

$$\epsilon = \frac{1}{V} \sum_{i=0}^{V-1} \frac{f_i - f_i^{eq}}{f_i^{eq}}, \quad (18)$$

where $\epsilon \approx Kn$ according to the Chapman-Enskog expansion²³. For large departures from the equilibrium state, such that $\epsilon > 10^{-2}$, the continuum limit assumption does not hold anymore, and the recovery of the macroscopic behavior of interest is then at risk²⁴. To prevent such an issue, one could refine the grid mesh depending on the value of ϵ , as proposed by Thorimbert et al.²⁵. Here, we prefer to damp high-order contributions, as soon as they appear in under resolved areas of the simulation domain, by adjusting the relaxation time accordingly to the local departure from the equilibrium state: $\tau(\epsilon) = \tau \alpha(\epsilon)$. As a simple proof of concept, α is chosen as a slowly increasing piecewise constant function of the local Knudsen number ϵ which, in the worst case, replaces the populations by equilibrium ($\epsilon \geq 1$):

$$\alpha = \begin{cases} 1, & \epsilon < 10^{-2} \\ 1.05, & 10^{-2} \leq \epsilon < 10^{-1} \\ 1.35, & 10^{-1} \leq \epsilon < 1 \\ 1/\tau, & \epsilon \geq 1 \end{cases} \quad (19)$$

where $1/\tau \approx 2$ in the context of high-Reynolds number flows, which ensures the well-posedness of α . This methodology amounts to artificially increasing the viscosity in areas of strong departure from the equilibrium state, and as such, is similar to both a subgrid scale model and a shock sensor. This information could also be used to better control the relaxation of high-order moments, similarly to the KBC collision model²⁶. Such an investigation will be presented in a future work.

Test cases. As a first validation, the generation and propagation of both rarefaction and shock waves is investigated through the simulation of a 1D Riemann problem, also known as Sod shock tube²⁷. The following initial setup is used: $(\rho_L, T_L) = (8, 10)$ and $(\rho_R, T_R) = (1, 1)$. Subscripts L and R stand for the left and the right states, respectively. The gas is considered at rest for both states, and the simulation domain is discretized along the x -direction using only $L_x = 400$ grid points. Corresponding

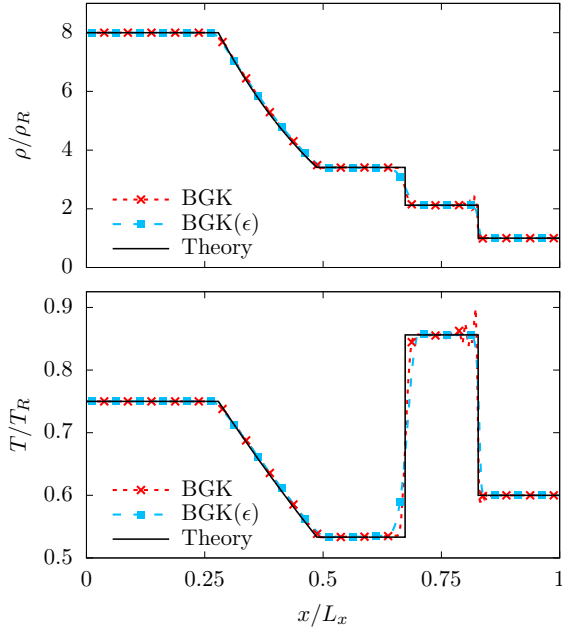


Figure 1. Sod shock tube for a diatomic gas (specific heat ratio $\gamma = 7/5$). Results obtained with $L = 400$ points using the standard BGK, and our version [BGK(ϵ)] are compared against theoretical curves, for $\tau_f = 0.57$ and 0.5 respectively.

results are compiled in Fig. 1 for both the standard BGK operator and our dynamic version based on Eq. (19). They prove the ability of the proposed model to simulate the generation and propagation of rarefaction and shock waves in a diatomic gas. Simulations are stable for relatively low values of the relaxation time ($\tau_f = 0.57$, $\text{Pr} = 1$), even with the standard BGK operator, while LBMs based on a polynomial discrete equilibrium usually require a large number of discrete velocities (37 in 2D) and more sophisticated collision models in order to achieve similar results⁷. Interestingly, the Knudsen number based relaxation times drastically improve the stability of the present model, allowing the simulation of 1D Riemann problem in the zero-viscosity limit ($\tau_f = 0.5$, $\text{Pr} = 1$), with an accuracy that competes with LBMs coupled with shock capturing techniques²⁴.

The next validation test consists of the simulation of the flow past a NACA0012 airfoil in the supersonic regime, and for a relatively high Reynolds number ($\text{Re} = 10^4$). Before moving to the results, it is worth noting that the standard BGK-LBM based on the equilibrium (11) led to stable simulations for Mach and Reynolds numbers up to 1.2 and 7500 respectively. These parameters are however insufficient for a comparison against data available in the literature^{15,28}, which is provided for $(\text{Ma}, \text{Re}) = (1.5, 10^4)$. Hence, the dynamic relaxation time based on the α function (19) was used to further extend the stability range of the present approach. The simulation domain is defined as $[n_x, n_y, n_z] = [8C, 8C, 1]$ with $C = 350$ points, n_j being the number of points in the j direction ($j = x, y$ or z), and centered around the leading edge of the airfoil. While the freestream conditions

are imposed on the left, top and bottom boundary conditions of the domain (by imposing $f_i = f_i^{eq}$ and $g_i = g_i^{eq}$), a (first-order) Neumann boundary condition is imposed at the (right) outlet. The no-slip boundary condition is imposed on the airfoil using half-way bounce-back.

The Mach number and the local Knudsen number ϵ fields are plotted in Fig. 2, as well as the pressure coefficient ($C_p = (p - p_\infty)/0.5\rho_\infty u_\infty^2$) profiles. The Mach number field highlights the main features of the flow: (1) primary strong bow shock upward the leading edge, (2) secondary weak shock close to the trailing edge, and (3) vortex shedding downward the airfoil. It qualitatively confirms the good behavior recovered thanks to the new equilibrium (11), as compared to results published in^{15,28}. Interestingly, the kinetic sensor ϵ is only active close to the aforementioned features, which allows to properly classify them in terms of departure from the equilibrium. This observation serves as a justification for the fact that the adaptive BGK operator leads to stable simulations through a local increase of the kinematic viscosity adapted to the flow features: high increase for both strong and weak shocks, moderate close to the airfoil, low in its wake, none in the rest of the domain. This indicates that one of the possible outcomes of such a sensor would be a better control over areas of the simulation domain where shock-capturing techniques, and/or subgrid scale models should be activated.

Eventually, the quantitative comparison of C_p profiles clearly shows that such a stabilization technique does not impact the level of accuracy reached by the present approach, even for relatively coarse grid meshes – as compared to¹⁶ where $C = 800$ grid points were used for the 343-shifted-velocity 5-constraints method – and using a very simple no-slip boundary condition. It is also worth noting that stable simulations were obtained for $\text{Re} = 10^9$ in under resolved conditions ($C = 200$ points). This further confirms the excellent properties of our Knudsen number based stabilization technique.

Possible extensions. In view of the drastic improvements obtained with the 13-moment based LBM (as compared to the 5-moment version), we strongly hypothesize that, by simply increasing the number of constraints used for the derivation of the exponential equilibrium, one could extend the present stability range to even higher Mach numbers, including potentially hypersonic conditions. In addition, by considering constraints based on other types of equilibria, this approach could be extended to simulate other types of flows (multiphase, magnetohydrodynamic, semi-classical, relativistic, etc) and physics (electromagnetism, quantum systems, etc). For example, this would be particularly suitable for semi-classical²⁹ and relativistic³⁰ LBMs, where a large number of constraints must be satisfied to recover the macroscopic behavior of interest, and current models use very large lattices.

Regarding the kinetic sensor, it only depends on the departure from equilibrium, and can correspondingly be extended to any type of physics. Furthermore, it could also

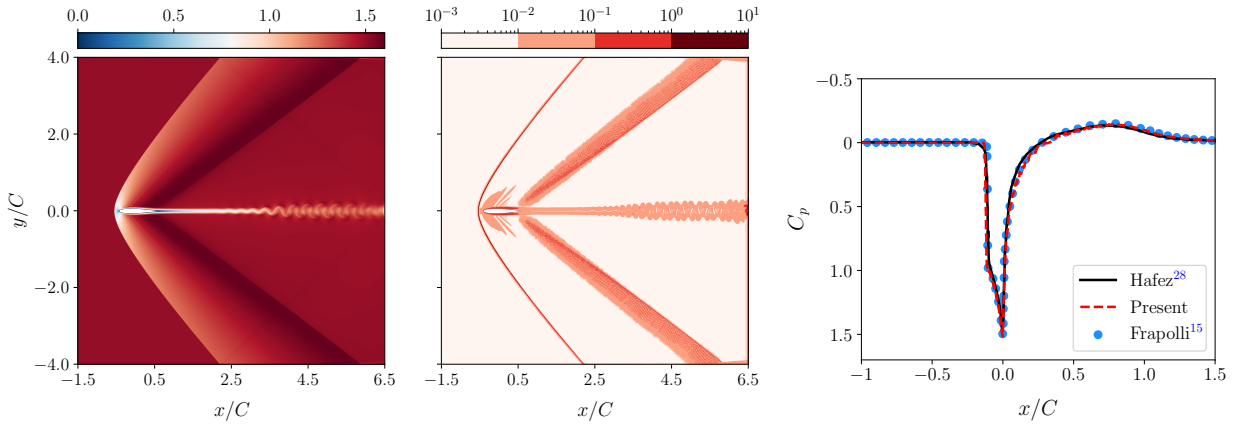


Figure 2. NACA0012 airfoil at $Ma = 1.5$ and $Re = 10^4$ using $C = 350$ points. From left to right: Mach number, local Knudsen number ϵ , and comparison of C_p distribution around the airfoil.

be used to identify underresolved areas where either a stabilization technique (subgrid scale models and/or shock capturing) or mesh refinement are required.

Acknowledgments. Useful discussions and scientific in-

put from Dr. Nicolò Frapolli, Dr. Orestis Malaspinas, and Dr. Dimitrios Kontaxakis, in the elaboration of the model presented in this paper, are gratefully acknowledged.

* Corresponding author: jonas.latt@unige.ch

¹ K. Huang, *Statistical Mechanics, 2nd Edition*, 2nd ed. (Wiley, 1987).

² X. Shan, X.-F. Yuan, and H. Chen, *J. Fluid Mech.* **550**, 413 (2006).

³ T. Krüger, H. Kusumaatmaja, A. Kuzmin, O. Shardt, G. Silva, and E. M. Viggien, *The Lattice Boltzmann Method: Principles and Practice* (Springer International Publishing, 2017).

⁴ S. Succi, *The Lattice Boltzmann Equation: For Complex States of Flowing Matter* (Oxford University Press, 2018).

⁵ Z. Guo and C. Shu, *Lattice Boltzmann Method and Its Applications in Engineering* (2013).

⁶ D. N. Siebert, L. A. Hegele, and P. C. Philippi, *Phys. Rev. E* **77**, 026707 (2008).

⁷ C. Coreixas, G. Wissocq, G. Puigt, J.-F. Boussuge, and P. Sagaut, *Phys. Rev. E* **96**, 033306 (2017).

⁸ X. Li, Y. Shi, and X. Shan, *Phys. Rev. E* **100**, 013301 (2019).

⁹ Q. Li, Y. L. He, Y. Wang, and W. Q. Tao, *Phys. Rev. E* **76**, 056705 (2007).

¹⁰ Y. Feng, P. Sagaut, and W.-Q. Tao, *Comput. Fluids* **131**, 45 (2016).

¹¹ X. Nie, X. Shan, and H. Chen, in *Aerospace Sciences Meetings*, Vol. 139 (American Institute of Aeronautics and Astronautics, 2009).

¹² E. Fares, M. Wessels, R. Zhang, C. Sun, N. Gopalaswamy, P. Roberts, J. Hoch, and H. Chen, *52nd AIAA Aerospace Sciences Meeting* **0952** (2014), 10.2514/6.2014-0952.

¹³ F. Renard, Y. Feng, J.-F. Boussuge, and P. Sagaut, (under review).

¹⁴ N. Frapolli, S. S. Chikatamarla, and I. V. Karlin, *Phys. Rev. E* **92**, 061301 (2015).

¹⁵ N. Frapolli, S. S. Chikatamarla, and I. V. Karlin, *Phys. Rev. E* **93**, 063302 (2016).

¹⁶ N. Frapolli, *Entropic lattice Boltzmann models for thermal*

and compressible flows, Ph.D. thesis, ETH-Zürich (2017).

¹⁷ A. Kogan, *J. Appl. Math. Mech.* **29**, 130 (1965).

¹⁸ S. Pressé, K. Ghosh, J. Lee, and K. A. Dill, *Rev. Mod. Phys.* **85**, 1115 (2013).

¹⁹ H. Struchtrup and M. Torrilhon, *Phys. Fluids* **15**, 2668 (2003).

²⁰ V. A. Rykov, *Fluid Dyn.* **10**, 959 (1975).

²¹ X. Nie, X. Shan, and H. Chen, *Phys. Rev. E* **77**, 035701 (2008).

²² W. H. Press, S. A. Teukolsky, W. T. Vetterling, and B. P. Flannery, *Numerical recipes: the art of scientific computing*, 3rd ed. (Cambridge University Press, 2007).

²³ S. Chapman and T. Cowling, *The Mathematical Theory of Non-uniform Gases: An Account of the Kinetic Theory of Viscosity, Thermal Conduction and Diffusion in Gases* (Cambridge University Press, 1970).

²⁴ C. Coreixas, *High-order extension of the recursive regularized lattice Boltzmann method*, Ph.D. thesis, INP Toulouse (2018).

²⁵ Y. Thorimbert, D. Lagrava, O. Malaspinas, B. Chopard, and J. Latt, “Automatic grid refinement criterion for lattice Boltzmann method,” (2019), submitted to Computers & Fluids.

²⁶ I. V. Karlin, F. Bösch, and S. S. Chikatamarla, *Phys. Rev. E* **90**, 031302 (2014).

²⁷ G. A. Sod, *J. Comput. Phys.* **27**, 1 (1978).

²⁸ M. Hafez and E. Wahba, *Comput. Fluids* **36**, 39 (2007).

²⁹ R. C. V. Coelho and M. M. Doria, *Comput. Fluids* **165**, 144 (2018).

³⁰ A. Gabbana, M. Mendoza, S. Succi, and R. Tripiccone, *Phys. Rev. E* **95**, 053304 (2017).